Anomalous Nernst and Hall effects in magnetized platinum and palladium

G. Y. Guo,[1,2,*] Q. Niu,[3,4] and N. Nagaosa[5,6]

[1]*Department of Physics, National Taiwan University, Taipei 10617, Taiwan*

[2]*Graduate Institute of Applied Physics, National Chengchi University, Taipei 11605, Taiwan*

[3]*International Center for Quantum Materials and Collaborative Innovation Center of Quantum Matter, Peking University, Beijing 100871, China*

[4]*Department of Physics, The University of Texas at Austin, Austin, Texas 78712, USA*

[5]*Department of Applied Physics, University of Tokyo, Tokyo 113-8656, Japan*

[6]*RIKEN Center for Emergent Matter Science (CEMS), Wako, Saitama 351-0198, Japan*

(Received 19 April 2014; revised manuscript received 28 May 2014; published 9 June 2014)

We study the anomalous Nernst effect (ANE) and anomalous Hall effect (AHE) in proximity-induced ferromagnetic palladium and platinum which is widely used in spintronics, within the Berry phase formalism based on the relativistic band-structure calculations. We find that both the anomalous Hall (σ^A_{xy}) and Nernst (α^A_{xy}) conductivities can be related to the spin Hall conductivity (σ^S_{xy}) and band exchange splitting (Δ_{ex}) by relations $\sigma^A_{xy} = \Delta_{ex}\frac{e}{\hbar}\sigma^S_{xy}(E_F)'$ and $\alpha^A_{xy} = -\frac{\pi^2}{3}\frac{k_B^2 T \Delta_{ex}}{\hbar}\sigma^s_{xy}(\mu)''$, respectively. In particular, these relations would predict that the σ^A_{xy} in the magnetized Pt (Pd) would be positive (negative) since the $\sigma^S_{xy}(E_F)'$ is positive (negative). Furthermore, both σ^A_{xy} and α^A_{xy} are approximately proportional to the induced spin magnetic moment (m_s) because the Δ_{ex} is a linear function of m_s. Using the reported m_s in the magnetized Pt and Pd, we predict that the intrinsic anomalous Nernst conductivity (ANC) in the magnetic platinum and palladium would be gigantic, being up to ten times larger than, e.g., iron, while the intrinsic anomalous Hall conductivity (AHC) would also be significant.

DOI: 10.1103/PhysRevB.89.214406 PACS number(s): 71.15.Rf, 72.15.Eb, 72.25.Ba, 75.47.−m

I. INTRODUCTION

Spin transport electronics (spintronics) has recently attracted enormous attention mainly because of its promising applications in information storage and processing and other electronic technologies [1,2]. Spin current generation, detection, and manipulation are three key issues in the emerging spintronics. Large intrinsic spin Hall effect (SHE) in platinum has recently been predicted [3] and observed (see Refs. [4] and [5], and references therein). In the SHE, a transverse spin current is generated in response to an electric field in a metal with relativistic electron interaction. The SHE enables us to generate and control spin current without magnetic field or magnetic materials, which would be an important step for spintronics. Furthermore, in the inverse spin Hall effect, a transverse voltage drop arises due to the spin current [6,7], and this allows us to detect spin current by measuring the Hall voltage. Therefore, platinum has been widely used as a spin current generator and detector in recent spin current experiments, such as spin Seebeck effect [8], spin pumping [9], and spin Hall switching [10], and plays a unique role in recent developments in spintronics.

Platinum is an enhanced paramagnet because its 5*d* band is partially filled with a large density of states (DOS) at the Fermi level (E_F) [$N(E_F) = \sim$1.74 states/eV/spin]. Consequently, it could become ferromagnetic with a significant spin magnetic moment when placed next to a ferromagnetic metal [11,12] or in low-dimensional structures such as an atomic bilayer on silver (001) surface [13] or a freestanding atomic chain [14,15]. Indeed, platinum was reported to possess a magnetic moment as large as ∼0.2 and ∼0.5 μ_B/atom in Ni/Pt and Fe/Pt multilayers [11,12], respectively. In a ferromagnetic metal, a transverse charge current would be generated in response to an electric field due to relativistic spin-orbit coupling (SOC), an effect known as the anomalous Hall effect (AHE) [16], discovered by Hall [17] long ago. Since the AHE is another archetypal spin-related transport phenomenon [16] and the SOC strength in Pt is large, it would be interesting to study the AHE in the proximity-induced ferromagnetic platinum. Furthermore, as pointed out in Ref. [18], the fact that the Hall voltage could be generated by both the AHE and inverse SHE in the magnetized platinum might complicate the detection of the pure spin current and also related phenomena using platinum. Therefore, it is important to understand the transport and magnetic properties of the magentized platinum.

In a ferromagnet, the Hall voltage could also arise when a thermal gradient instead of an electric field is applied. This phenomenon, again due to the relativistic SOC, is referred to as the anomalous Nernst effect (ANE) [19]. Interestingly, the ANE could be used as a probe of the vortex phase in type-II superconductors [20] and has been receiving considerable attention in recent years [21–28]. In this context, it would be interesting to study the ANE in the proximity-induced ferromagnetic platinum. On the other hand, spin Seebeck effect (another thermal phenomenon), which refers to the generation of a spin-motive force in a ferromagnet by a temperature gradient, has recently attracted considerable attention [8,29,30]. Again, this effect is usually measured as a transverse voltage in a nonmagnetic metal such as Pt in contact with the ferromagnet via the inverse SHE [8]. Clearly, if the metal is magnetized due to the magnetic proximity effect, the ANE would contribute to the measured Hall voltage too. In this connection, it is imperative to understand the ANE in the magnetized platinum.

Palladium is isoelectronic to platinum and thus has an electronic structure similar to that of Pt except a smaller SOC

*gyguo@phys.ntu.edu.tw

strength (see, e.g., Refs. [3] and [31], and references therein). For example, like Pt, Pd also has a large intrinsic spin Hall conductivity (SHC) [31] and is a highly enhanced paramagnetic metal with a large $N(E_F) = \sim 2.69$ states/eV/spin. In fact, palladium possesses the largest paramagnetic susceptibility of 567×10^{-6} emu/mole among the nonmagnetic metals [32] and is usually considered to be nearly ferromagnetic. It could become ferromagnetic when placed next to a ferromagnetic metal [33,34] or fabricated as an atomic bilayer on silver (001) surface [13] or a freestanding atomic chain [15]. Recently, the AHE was observed in the Pd film on an yttrium iron garnet (YIG) [35]. Surprisingly, it was reported that the intrinsic anomalous Hall conductivity (AHC) in the Pd film on the YIG layer has a sign opposite to that for the Pt/YIG bilayer [35]. This indicates that the AHC in a magnetized nonmagnetic metal does not simply scale with the SOC strength. One would then ask what determines the AHC in the magnetized metals.

In this paper, therefore, we study the AHE and ANE in the proximity-induced ferromagnetic platinum and palladium within the Berry phase formalism [36] based on first-principles relativistic band-structure calculations. We also perform analytic calculations to identify possible relations between the SHC in a nonmagnetic metal and the AHC in the corresponding magnetized metal. The rest of this paper is organized as follows. In the next section, we briefly describe the Berry phase formalism for calculating the AHC and ANC as well as the computational details. In Sec. III, the calculated AHC and ANC will be presented. Finally, the conclusions drawn from this work will be summarized in Sec. IV.

II. THEORY AND COMPUTATIONAL DETAILS

The anomalous Hall conductivity and anomalous Nernst conductivity (ANC) are calculated by using the Berry-phase formalism [36]. Within this Berry-phase formalism, the AHC is simply given as a Brillouin zone (BZ) integration of the Berry curvature for all the occupied bands,

$$\sigma_{xy}^{A} = -\frac{e^2}{\hbar}\sum_{n}\int_{\mathrm{BZ}}\frac{d\mathbf{k}}{(2\pi)^3} f_{\mathbf{k}n}\Omega_{n}^{z}(\mathbf{k}),$$
$$\Omega_{n}^{z}(\mathbf{k}) = -\sum_{n'\neq n}\frac{2\mathrm{Im}[\langle \mathbf{k}n|v_x|\mathbf{k}n'\rangle\langle \mathbf{k}n'|v_y|\mathbf{k}n\rangle]}{(\epsilon_{\mathbf{k}n}-\epsilon_{\mathbf{k}n'})^2}, \quad (1)$$

where $f_{\mathbf{k}n}$ and Ω_n^z are the Fermi distribution function and the Berry curvature for the nth band at $\mathbf{k}$, respectively [37]. Similarly, the ANC can be written as

$$\alpha_{xy}^{A} = \frac{1}{T}\frac{e}{\hbar}\sum_{n}\int_{\mathrm{BZ}}\frac{d\mathbf{k}}{(2\pi)^3} f_{\mathbf{k}n}\Omega_{n}^{z}(\mathbf{k}) \times [(\epsilon_{\mathbf{k}n}-\mu) f_{\mathbf{k}n} + k_B T \ln(1+e^{-\beta(\epsilon_{\mathbf{k}n}-\mu)})], \quad (2)$$

where μ is the chemical potential and k_B is the Boltzmann constant [22].

The proximity-induced ferromagnetic platinum and palladium are investigated by the constrained spin-density-functional theory with the local-density approximation to the exchange-correlation potential [38]. Spin-polarized self-consistent scalar-relativistic electronic structure calculations with the spin magnetic moment fixed to specified values are performed. Using the resultant self-consistent charge densities, the fully relativistic band structures are then calculated for the AHC and ANC calculations. The highly accurate all-electron full-potential linearized augmented plane wave (FLAPW) method, as implemented in the WIEN2K code [39], is used. The experimental lattice constants $a = 3.92$ and 3.89 (Å) are used, respectively, for Pt and Pd. In both cases, the muffin-tin sphere radius (R_{mt}) of 2.5 a.u. is adopted. The wave function, charge density, and potential are expanded in terms of the spherical harmonics inside the muffin-tin spheres and the cutoff angular moment ($L_{\max}$) used is 10, 6, and 6, respectively. The wave function outside the muffin-tin sphere is expanded in terms of the augmented plane waves (APWs) and a large number of APWs (about 70 APWs per atom, i.e., the maximum size of the crystal momentum $K_{\max} = 9/R_{mt}$) are included in the present calculations. The tetrahedron method is used for the BZ integration [40]. To obtain accurate ground-state properties, a fine $21 \times 21 \times 21$ grid of 11 616 k points in the first BZ is used. For the AHC and ANC calculations, a very fine grid of 258 156 k points on the magnetic irreducible wedge (1/16 BZ) in the BZ is used. This is equivalent to a large number of k points of ~4 000 000 in the full BZ, and corresponds to the division of the ΓX line into 70 intervals. Comparison with test calculations with a denser grid of 381 915 k points (80 divisions of the ΓX line) indicates that the calculated AHC and ANC converge to within a few %.

III. RESULTS AND DISCUSSION

The relativistic band structure and also AHC (σ_{xy}^{A}) as a function of the Fermi energy (E_F) for the magnetized platinum and palladium with the spin magnetic moment $m_s = 0.1\ \mu_B$/atom are displayed in Figs. 1 and 2, respectively. All Kramer-degenerate bands in nonmagnetic platinum (see Fig. 1 in [3]) and palladium (see Fig. 1 in [31]) are now exchange-split

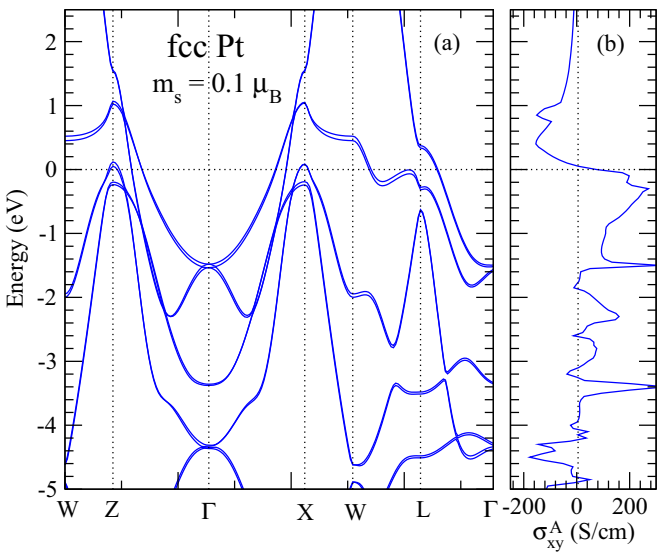

FIG. 1. (Color online) (a) Relativistic band structure and (b) anomalous Hall conductivity (AHC) of the magnetized platinum with a spin magnetic moment of 0.1 μ_B/atom. The horizontal dotted line at the zero energy indicates the Fermi level.

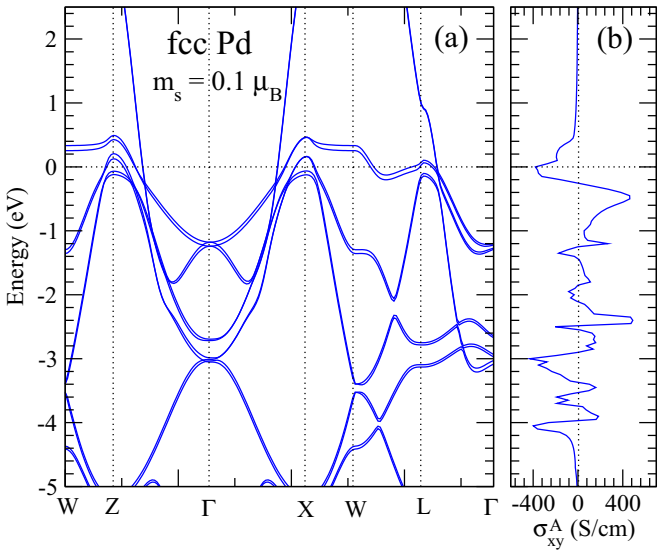

FIG. 2. (Color online) (a) Relativistic band structure and (b) anomalous Hall conductivity of the magnetized palladium with a spin magnetic moment of 0.1 μ_B/atom. The horizontal dotted line at the zero energy indicates the Fermi level.

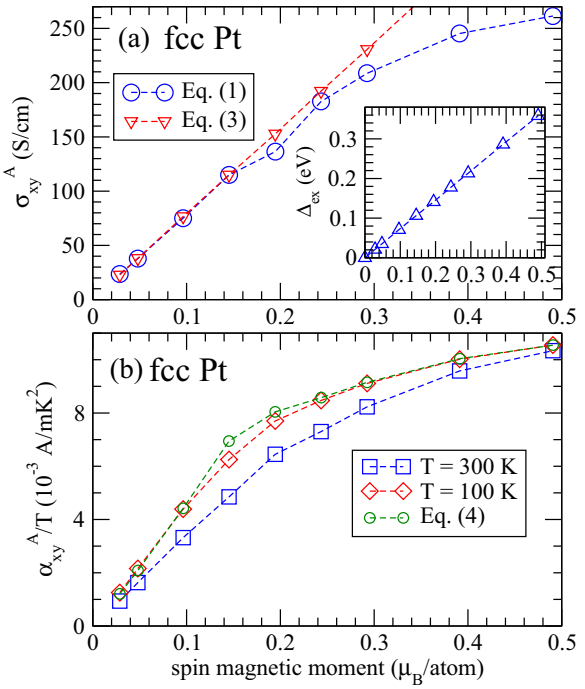

FIG. 3. (Color online) (a) Anomalous Hall conductivity (σ^A_{xy}) and (b) anomalous Nernst conductivity (α^A_{xy}) as a function of the induced spin magnetic moment (m_s) in platinum. Exchange splitting (Δ_{ex}) is displayed as a function of m_s in the inset in (a). In (b), T denotes temperature.

due to the induced magnetization in the magnetized Pt and Pd. This is clearly visible for the d-dominated bands [i.e., energy bands below 1.0 eV in Fig. 1(a) or 0.5 eV in Fig. 2(a)] since the ferromagnetism is mainly caused by the exchange interaction among the d electrons. The band spin-splittings are largest in the flat bands of almost pure d character such as the bands around 0.5 eV (0.3 eV) in the vicinity of the W point in Fig. 1(a) [Fig. 2(a)].

A. Anomalous Hall effect

Figures 3 and 4 show the calculated AHC and ANC (α^A_{xy}) as well as the exchange splitting (Δ_{ex}) as a function of the induced spin magnetic moment (m_s) in platinum and palladium, respectively. Δ_{ex} refers to the splitting of the spin-up and spin-down bands, and we calculate Δ_{ex} as the spin splitting of the scalar-relativistic bands above the Fermi level at the W point [Figs. 1(a) and 2(a)]. First of all, it is clear from Figs. 3 and 4 that the calculated σ^A_{xy} and Δ_{ex} increase monotonically with m_s. In fact, Δ_{ex} is almost perfectly proportional to m_s, while the amplitude of the σ^A_{xy} increases linearly with m_s for small m_s values up to 0.30 and 0.25 μ_B/atom for Pt and Pd, respectively.

Second, the AHC is large. In particular, the magnitude of the AHC per μ_B (σ^A_{xy}/m_s) for $m_s \leqslant 0.25$ μ_B/atom in Pt and Pd is, respectively, ~790 and 3500 S/(cm μ_B), being much larger than that of ~360 S/(cm μ_B) in iron [37]. Interestingly, the ratio σ^A_{xy}/m_s for Pt is smaller than that for Pd, indicating that the AHC in a proximity-induced ferromagnetic metal is not necessarily correlated with the SOC strength. Third, the sign of the AHC in Pt is opposite to that in Pd, being in good agreement with the recent experiments on the Pt/YIG and Pd/YIG bilayers [35].

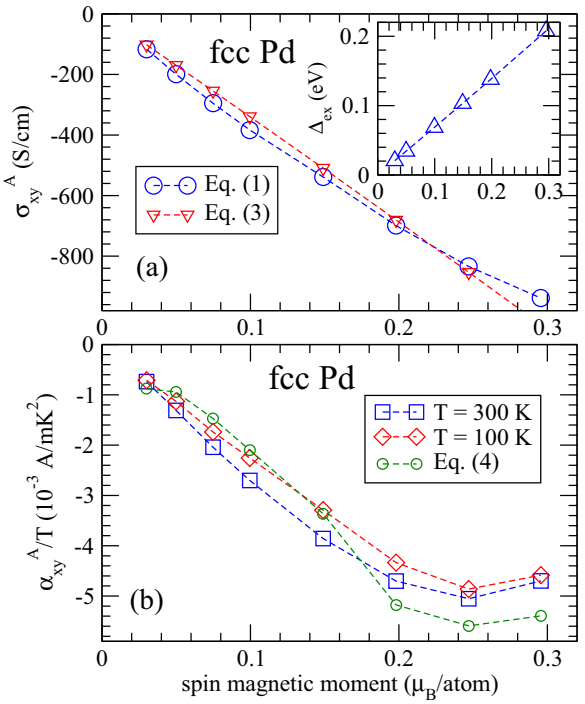

FIG. 4. (Color online) (a) Anomalous Hall conductivity (σ^A_{xy}) and (b) anomalous Nernst conductivity (α^A_{xy}) as a function of the induced spin magnetic moment (m_s) in palladium. Exchange splitting (Δ_{ex}) is displayed as a function of m_s in the inset in (a). In (b), T denotes temperature.

B. Correlation between anomalous and spin Hall conductivities

In order to gain insight into the key factors that determine the AHC in a magnetized nonmagnetic metal, let us consider the two-current model to connect the conductivities for the different sorts of Hall effects. Within the two-current model approximation, σ^A_{xy} and σ^S_{xy} can be written as [41–43] $\sigma^A_{xy}(E) = \sigma^{\uparrow}_{xy}(E) + \sigma^{\downarrow}_{xy}(E)$ and $-2\frac{\hbar}{e}\sigma^S_{xy}(E) = \sigma^{\uparrow}_{xy}(E) - \sigma^{\downarrow}_{xy}(E)$, where $\sigma^{\uparrow}_{xy}$ and $\sigma^{\downarrow}_{xy}$ are the spin-up and spin-down Hall conductivities, respectively. In a nonmagnetic metal, the spin magnetic moment $m_s = 0$ and thus, $\sigma^A_{xy} = 0$. In the magnetized metal, $\sigma^A_{xy}(E) = \sigma^{\uparrow}_{xy}(E - \frac{1}{2}\Delta_{ex}) + \sigma^{\downarrow}_{xy}(E + \frac{1}{2}\Delta_{ex}) \approx \sigma^{\uparrow}_{xy}(E) - \frac{1}{2}\Delta_{ex}\sigma^{\uparrow}_{xy}(E)' + \sigma^{\downarrow}_{xy}(E) + \frac{1}{2}\Delta_{ex}\sigma^{\downarrow}_{xy}(E)'$, where Δ_{ex} is the exchange splitting and is proportional to m_s, as shown in the inset in Figs. 3(a) and 4(a). Therefore, we find

$$\sigma^A_{xy}(E_F) \approx \Delta_{ex}\frac{e}{\hbar}\sigma^S_{xy}(E_F)'. \tag{3}$$

Equation (3) tells us that the AHC is proportional to the energy derivative of the spin Hall conductivity [σ^S_{xy}] as well as the exchange splitting (Δ_{ex}). Interestingly, the SOC strength does not appear explicitly in Eq. (3), contrary to conventional wisdom. We notice that platinum and palladium have similar SHC-versus-energy [$\sigma^S_{xy}(E)$] curves which have a prominent peak near the E_F (see Fig. 1 in both [3] and [31]). However, the E_F falls on the uphill side of the peak in Pt [3] but on the downhill side of the peak in Pd [31], resulting in the positive $\sigma^S_{xy}(E_F)'$ for Pt and negative $\sigma^S_{xy}(E_F)'$ for Pd. This, together with Eq. (3), naturally explains why both the calculated and observed AHCs in Pt and Pd have opposite signs.

To examine quantitatively the validity of Eq. (3), here we repeat the calculations of the SHC for Pt [3] and Pd [31] but using the more accurate FLAPW method with the same computational details as described already in Sec. II. The calculated SHC for Pt and Pd as a function of energy is displayed in Fig. 5(a). The σ^S_{xy} at the E_F is 2200 $(\hbar/e)$S/cm for Pt and 1242 $(\hbar/e)$S/cm for Pd, being in good agreement with the corresponding results calculated previously using the linear muffin-tin orbital method with the atomic sphere approximation [3,31]. We then evaluate numerically the energy derivative of the SHC using the $\sigma^S_{xy}(E)$ displayed in Fig. 5. We obtain $\sigma^S_{xy}(E_F)' = 1081$ and -4245 $(\hbar/e)$S/cm eV for Pt and Pd, respectively. Figures 3(a) and 4(a) also show the σ^A_{xy} evaluated using Eq. (3) together with the calculated $\sigma^S_{xy}(E_F)'$ and Δ_{ex}. It is clear that Eq. (3) holds very well for small m_s up to $\sim$0.25 μ_B/atom for Pt and Pd [Figs. 3(a) and 4(a)].

We have also calculated the SHC in the magnetized Pt and Pd metals. The calculated SHC for Pt and Pd is shown as a function of the spin magnetic moment in Fig. 5(b). In both Pt and Pd, the SHC initially increases with m_s up to $\sim$0.1 μ_B/atom and then decreases slowly as m_s further increases [Fig. 5(b)]. Nevertheless, the SHC for both Pt and Pd remains in the same order of magnitude all the way up to $m_s = 0.5$ μ_B/atom.

The validity of Eq. (3) may be understood at the microscopic level. The two-current model can be derived from an approximation in which the spin-flipping part of the SOC is ignored. The spin-conserving part of the SOC can still lead to nontrivial results on the transverse transport coefficients.

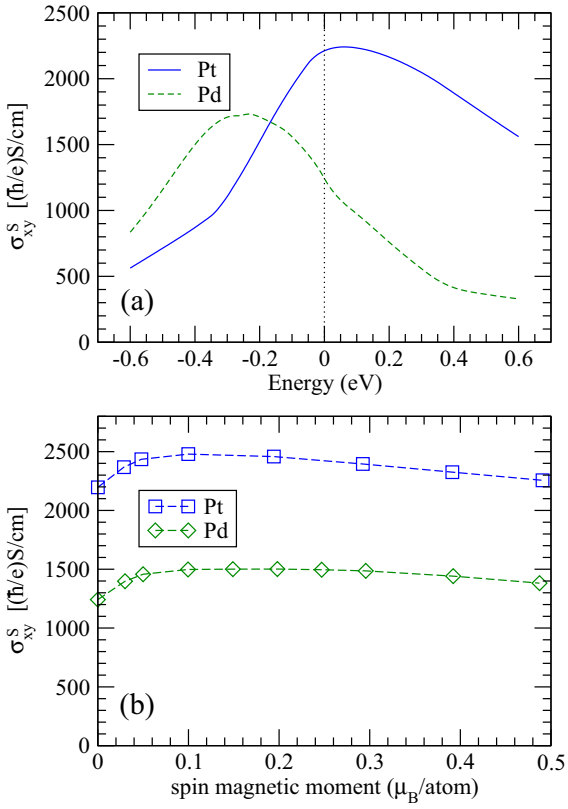

FIG. 5. (Color online) (a) Spin Hall conductivity (σ^S_{xy}) as a function of energy in nonmagnetic Pt and Pd metals. The vertical dotted line at 0 eV indicates the Fermi energy (E_F). $\sigma^S_{xy}(E_F) = 2200$ and 1242 $(\hbar/e)$S/cm for Pt and Pd, respectively. $\sigma^S_{xy}(E_F)' = 1081$ and -4245 $(\hbar/e)$S/cm eV for Pt and Pd, respectively. (b) Spin Hall conductivity as a function of the induced spin magnetic moment (m_s) in magnetized Pt and Pd metals.

This nonflip approximation can be justified for crystals with inversion symmetry and in the limit of zero magnetization. This is because Kramer's theorem implies a twofold degeneracy of the band structure at general k points even in the presence of the SOC. The SOC term in the Hamiltonian, being symmetric under spatial inversion and time reversal, must behave as a constant within the degenerate space. Therefore, it must also commute with the representation of the spin operator within the twofold degenerate space. In the presence of a small magnetization, the degenerate bands are split to first order in the Zeeman energy according to the representation of the spin operator within each of the original degenerate space. Not being able to mix these split levels directly, the spin-flip part of the SOC term in the Hamiltonian can be safely discarded, because its residual effect must be of second order (in a process going out and back to the degenerate space).

C. Anomalous Nernst effect

Figures 3(b) and 4(b) indicate first that the anomalous Nernst conductivity α^A_{xy} increases monotonically with the spin moment m_s for m_s up to at least 0.5 μ_B/atom in Pt and for m_s up to 0.25 μ_B/atom in Pd. Like σ^A_{xy}, α^A_{xy} is approximately proportional to m_s for $m_s \leqslant \sim 0.20\,\mu_B$/atom in both Pt and Pd.

Second, the calculated α_{xy}^A is large, especially in Pt [Fig. 3(b)]. In fact, α_{xy}^A for Pt at $m_s \geqslant 0.15\ \mu_B$/atom could be ten times larger than the intrinsic α_{xy}^A [$\alpha_{xy}^A/\mathrm{T} = 0.51 \times 10^{-3}$ A/(m K^2) at $T = 293$ K] of iron [27]. The magnitude of α_{xy}^A for Pd for $m_s \geqslant 0.05\ \mu_B$/atom is also several times larger than that of iron [27].

At low temperatures, Eq. (2) can be simplified as the Mott relation,

$$\alpha_{xy}^A = -\frac{\pi^2}{3}\frac{k_B^2 T}{e}\sigma_{xy}^A(\mu)', \tag{4}$$

which relates the ANC to the AHC. Therefore, it is not surprising that the magnetized platinum has a very large α_{xy}^A since the E_F is located on the steep slope of $\sigma_{xy}^A(E)$ [Fig. 1(b)], resulting in a large energy derivative of $\sigma_{xy}^A(E)$ at E_F. In Figs. 1(b) and 2(b), the α_{xy}^A calculated using the Mott relation [Eq. (4)] is displayed as a function of the induced m_s. Clearly, α_{xy}^A calculated directly [Eq. (2)] and using the Mott relation at $T = 100$ K are in good agreement with each other for Pt [see Fig. 3(b)] and also for $m_s \leqslant 0.15\ \mu_B$/atom for Pd [see Fig. 4(b)]. On the other hand, α_{xy}^A at $T = 300$ K calculated directly differs noticeably from that from the Mott relation, indicating that $T = 300$ K cannot be considered as a low temperature in this context.

Differentiating Eq. (3) and substituting the result into Eq. (4), we find

$$\alpha_{xy}^A/T = -\frac{\pi^2}{3}\frac{k_B^2 \Delta_{ex}}{\hbar}\sigma_{xy}^s(\mu)''. \tag{5}$$

Equations (3) and (4) indicate that for small m_s, both the AHC and ANC are proportional to the exchange-splitting. As mentioned above, the exchange-splitting is almost a perfect linear function of m_s, and hence this explains why both the σ_{xy}^A and α_{xy}^A are approximately proportional to m_s. Furthermore, this suggests that the σ_{xy}^A and α_{xy}^A are proportional to each other for small m_s, as shown in Figs. 3 and 4. Therefore, we can rewrite Eq. (3) as

$$\sigma_{xy}^A(E_F) \approx \left[\frac{e}{\hbar}\frac{\Delta_{ex}(m_s^0)}{m_s^0}\sigma_{xy}^S(E_F)'\right]m_s = \beta m_s, \tag{6}$$

where constant β can be determined solely by first-principles calculations for a certain spin moment m_s^0. In the present work, we find that $\beta = 788$ S/cm/μ_B for Pt and $\beta = -2921$ S/cm/μ_B for Pd. Similarly, we can rewrite Eq. (4) as

$$\alpha_{xy}^A/T \approx -\left[\frac{\pi^2}{3}\frac{k_B^2 \Delta_{ex}(m_s^0)}{\hbar m_s^0}\sigma_{xy}^S(E_F)''\right]m_s = \gamma m_s. \tag{7}$$

And using the results of the first-principles calculations, we obtain that constant $\gamma = 0.034$ A/(m K$^2\mu_B$) for Pt and $\gamma = -0.027$ A/(m K$^2\mu_B$) for Pd.

IV. CLOSING REMARKS

Recently, the possible magnetic proximity-induced spin moment in Pt films in the Pt/YIG bilayers was measured by magnetic x-ray circular dichroism experiments [44], and m_s was found to be 0.054 μ_B/atom at 300 K and 0.076 μ_B/atom at 20 K. Using $m_s = 0.05\ \mu_B$/atom together with Eqs. (6) and (7), we can estimate the intrinsic AHC and ANC for the Pt film to be $\sigma_{xy}^A = 40$ S/cm and $\alpha_{xy}^A = 0.51$ A/(m K^2) ($T = 300$ K). The anomalous Seebeck coefficient $E_y/(-\partial_x T) = \rho_{xx}(\alpha_{xy} - S\sigma_{xy})$ where $S = \alpha_{xx}/\sigma_{xx}$ is the ordinary Seebeck coefficient. At $T = 300$ K, $\rho_{xx} = 10.8\ \mu\Omega$ cm and $S = -11.28\ \mu$V/K (see Refs. [45] and [46]). Resultantly, $E_y/(-\partial_x T) = 0.058\ \mu$V/K. Using the sample sizes and the temperature gradient in the Pt/YIG bilayers [47,48], one would obtain the Hall voltage due to the ANE in the order of $\sim$0.1 μV, being comparable with the Hall voltage ($\sim$0.1 μV in Au/YIG and $\sim$1.0 μV in Pt/YIG) produced by the spin Seebeck effect via the inverse spin Hall effect.

ACKNOWLEDGMENTS

G.Y.G. acknowledges support from the Ministry of Science and Technology, the Academia Sinica Thematic Research Program, and NCTS of Taiwan, and thanks Shang-Fan Lee and Shiming Zhou for stimulating discussions. G.Y.G. also acknowledges partial support from NBRPC (Grants No. 2012CB921300 and No. 2013CB921900), and NSFC (Grant No. 91121004) during his visit at Peking University. Q.N. was supported in part by DOE-DMSE (Grant No. DE-FG03-02ER45958) and the Welch Foundation (Grant No. F-1255).

[1] G. A. Prinz, Science **282**, 1660 (1998); S. A. Wolf, D. D. Awschalom, R. Chtchelkanova, and D. M. Treger, *ibid.* **294**, 1488 (2001).
[2] I. Zutic, J. Fabianm, and S. D. Sarma, Rev. Mod. Phys. **76**, 323 (2004).
[3] G. Y. Guo, S. Murakami, T.-W. Chen, and N. Nagaosa, Phys. Rev. Lett. **100**, 096401 (2008).
[4] Z. Feng, J. Hu, L. Sun, B. You, D. Wu, J. Du, W. Zhang, A. Hu, Y. Yang, D. M. Tang, B. S. Zhang, and H. F. Ding, Phys. Rev. B **85**, 214423 (2012).
[5] A. Hoffman, IEEE Trans. Mag. **49**, 5172 (2013).
[6] S. O. Valenzuela and M. Tinkham, Nature (London) **442**, 176 (2006).
[7] E. Saitoh, M. Ueda, H. Miyajima, and G. Tatara, Appl. Phys. Lett. **88**, 182509 (2006).
[8] K. Uchida, S. Takahashi, K. Harii, J. Ieda, W. Koshibae, K. Ando, S. Maekawa, and E. Saitoh, Nature (London) **455**, 778 (2008).
[9] Y. Kajiwara, K. Harii, S. Takahashi, J. Ohe, K. Uchida, M. Mizuguchi, H. Umezawa, H. Kawai, K. Ando, K. Takanashi, S. Maekawa, and E. Saitoh, Nature (London) **464**, 262 (2010).
[10] I. M. Miron, K. Garello, G. Gaudin, P.-J. Zermatten, M. V. Costache, S. Auffret, S. Bandiera, B. Rodmacq, A. Schuhl, and P. Gambardella, Nature (London) **476**, 189 (2011).
[11] F. Wilhelm, P. Poulopoulos, G. Ceballos, H. Wende, K. Baberschke, P. Srivastava, D. Benea, H. Ebert, M. Angelakeris, N. K. Flevaris, D. Niarchos, A. Rogalev, and N. B. Brookes, Phys. Rev. Lett. **85**, 413 (2000).
[12] W. J. Antel, Jr., M. M. Schwickert, T. Lin, W. L. O'Brien, and G. R. Harp, Phys. Rev. B **60**, 12933 (1999).

[13] S. Blügel, Phys. Rev. B **51**, 2025 (1995).
[14] A. Smogunov, A. Dal Corso, A. Delin, R. Weht, and E. Tosatti, Nat. Nanotechnol. **3**, 22 (2008).
[15] J.-C. Tung and G. Y. Guo, Phys. Rev. B **81**, 094422 (2010).
[16] N. Nagaosa, J. Sinova, S. Onoda, A. H. MacDonald, and N. P. Ong, Rev. Mod. Phys. **82**, 1539 (2010).
[17] E. H. Hall, Philos. Mag. B **12**, 157 (1881).
[18] S. Y. Huang, X. Fan, D. Qu, Y. P. Chen, W. G. Wang, J. Wu, T. Y. Chen, J. Q. Xiao, and C. L. Chien, Phys. Rev. Lett. **109**, 107204 (2012).
[19] W. Nernst, Ann. Phys. **267**, 760 (1887).
[20] Z. A. Xu, N. P. Ong, Y. Wang, T. Kakeshita, and S. Uchida, Nature (London) **406**, 486 (2000).
[21] W.-L. Lee, S. Watauchi, V. L. Miller, R. J. Cava, and N. P. Ong, Phys. Rev. Lett. **93**, 226601 (2004).
[22] D. Xiao, Y. Yao, Z. Fang, and Q. Niu, Phys. Rev. Lett. **97**, 026603 (2006).
[23] T. Miyasato, N. Abe, T. Fujii, A. Asamitsu, S. Onoda, Y. Onose, N. Nagaosa, and Y. Tokura, Phys. Rev. Lett. **99**, 086602 (2007).
[24] D. L. Bergman and V. Oganesyan, Phys. Rev. Lett. **104**, 066601 (2010).
[25] T. Yokoyama and S. Murakami, Phys. Rev. B **83**, 161407 (2011).
[26] S. Y. Huang, W. G. Wang, S. F. Lee, J. Kwo, and C. L. Chien, Phys. Rev. Lett. **107**, 216604 (2011).
[27] J. Weischenberg, F. Freimuth, S. Blügel, and Y. Mokrousov, Phys. Rev. B **87**, 060406 (2013).
[28] M. Schmid, S. Srichandan, D. Meier, T. Kuschel, J.-M. Schmalhorst, M. Vogel, G. Reiss, C. Strunk, and C. H. Back, Phys. Rev. Lett. **111**, 187201 (2013).
[29] K. Uchida, Nat. Mater. **9**, 894 (2010).
[30] C. M. Jaworski, J. Yang, S. Mack, D. D. Awschalom, J. P. Heremans, and R. C. Myers, Nat. Mater. **9**, 898 (2010).
[31] G. Y. Guo, J. Appl. Phys. **105**, 07C701 (2009).
[32] R. Huguenin, G. P. Pells, and D. N. Baldock, J. Phys. F: Metal Phys. **1**, 281 (1971).
[33] Z. Celinski, B. Heinrich, J. F. Cochran, W. B. Muir, A. S. Arrott, and J. Kirschner, Phys. Rev. Lett. **65**, 1156 (1990).
[34] J. R. Childress *et al.*, J. Magn. Magn. Mater. **130**, 13 (1994).
[35] X. Zhou, L. Ma, Z. Shi, and S. M. Zhou, arXiv:1309.4841.
[36] D. Xiao, M.-C. Chang, and Q. Niu, Rev. Mod. Phys. **82**, 1959 (2010).
[37] Y. Yao, L. Kleinman, A. H. MacDonald, J. Sinova, T. Jungwirth, D.-S. Wang, E. Wang, and Q. Niu, Phys. Rev. Lett. **92**, 037204 (2004).
[38] S. H. Vosko, L. Wilk, and M. Nusair, Can. J. Phys. **58**, 1200 (1980).
[39] P. Blaha, K. Schwarz, G. Madsen, D. Kvasnicka, and J. Luitz, *WIEN2K, An Augmented Plane Wave Local Orbitals Program for Calculating Crystal Properties* (Technische University Wien, Austria, 2002).
[40] O. Jepson and O. K. Anderson, Solid State Commun. **9**, 1763 (1971).
[41] J.-C. Tung, H.-R. Fuh, and G. Y. Guo, Phys. Rev. B **86**, 024435 (2012).
[42] J.-C. Tung and G. Y. Guo, New J. Phys. **15**, 033014 (2013).
[43] Note that in Refs. [41] and [42], $2\frac{\hbar}{e}\sigma_{xy}^{S} = \sigma_{xy}^{\uparrow} - \sigma_{xy}^{\downarrow}$ in Eq. (5) and Eq. (2b), respectively, should be $-2\frac{\hbar}{e}\sigma_{xy}^{S} = \sigma_{xy}^{\uparrow} - \sigma_{xy}^{\downarrow}$. Consequently, the signs of the spin-up and spin-down Hall conductivities ($\sigma_{xy}^{\uparrow}$ and $\sigma_{xy}^{\downarrow}$) as well as the spin polarization of the Hall current (P^{H}) listed in Tables I and II in Refs. [41] and [42] should be reversed.
[44] Y. M. Lu, Y. Choi, C. M. Ortega, X. M. Cheng, J. W. Cai, S. Y. Huang, L. Sun, and C. L. Chien, Phys. Rev. Lett. **110**, 147207 (2013).
[45] *Metals: Electronic Transport Phenomena*, Landolt-Börnstein, New Series, Vol. 15, Pt. a, edited by J. Bass and K. H. Fischer (Springer-Verlag, Berlin, 1982).
[46] *Metals: Electronic Transport Phenomena*, Landolt-Börnstein, New Series, Vol. 15, Pt. b, edited by J. Bass, J. S. Dugdale, C. L. Foiles, and A. Myers (Springer-Verlag, Berlin, 1982).
[47] D. Qu, S. Y. Huang, J. Hu, R. Wu, and C. L. Chien, Phys. Rev. Lett. **110**, 067206 (2013).
[48] T. Kikkawa, K. Uchida, Y. Shiomi, Z. Qiu, D. Hou, D. Tian, H. Nakayama, X.-F. Jin, and E. Saitoh, Phys. Rev. Lett. **110**, 067207 (2013).